

Constructing SiO₂-Supported Atomically Dispersed Platinum Catalysts with Single-Atom and Atomic Cluster Dual Sites to Tame Hydrogenation Performance

Hao Xu,[◆] Dong Lin,[◆] Jie Shi,[◆] Zhengxing Lv,[◆] Xinshuo Zhao, Linge Ning, Jiao Xiao, Lin Cui, Jian Zhang, Juncong Yuan, Xiang Feng,* Yong Qin,* and Jiankang Zhang*



Cite This: *JACS Au* 2025, 5, 250–260



Read Online

ACCESS |



Metrics & More



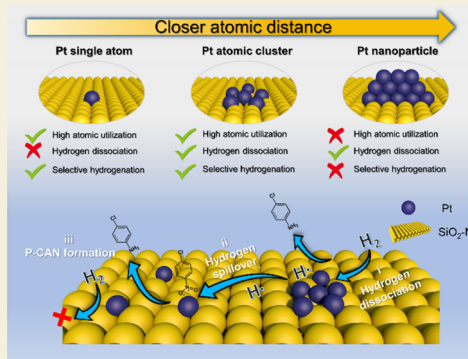
Article Recommendations



Supporting Information

ABSTRACT: Construction and optimization of stable atomically dispersed metal sites on SiO₂ surfaces are important yet challenging topics. In this work, we developed the amino group-assisted atomic layer deposition strategy to deposit the atomically dispersed Pt on SiO₂ support for the first time, in which the particle size and ratio of Pt entities from single atom (Pt₁) to atomic cluster (Pt_n) and nanoparticle (Pt_n) on the SiO₂ surface were well modulated. We demonstrated the importance of dual-site synergy for optimizing the activity of single-atom catalysts. The Pt_{1+n}/SiO₂-N catalysts with the coexistence of Pt₁ and Pt_n showed excellent activity and optimized selectivity (99% for haloanilines) in halonitrobenzenes hydrogenation, while Pt₁/SiO₂-N catalysts were almost inactive in the reaction. Mechanism investigation indicates that the Pt_n site is beneficial for H₂ dissociation, and the Pt₁ site is energetically favorable for adsorption of the nitro group to complete the selective hydrogenation, which synergistically contributes to the optimized catalytic performances. This study provides a new strategy for constructing atomically dispersed metal species over the SiO₂ support and demonstrates the significance of the synergy of dual active sites for enhancing the catalytic efficiency.

KEYWORDS: atomic layer deposition, Pt single atoms and clusters, dual active sites, synergy, selective hydrogenation



INTRODUCTION

Heterogeneous catalysts with maximized metal dispersion, optimal intrinsic activity per metal atom, and well-defined coordination structure are the long-term pursuit in catalysis.^{1–3} Single-atom catalysts (SACs), as an emerging catalytic material system, have drawn extensive attention in many applications due to their ultimate atomic utilization, uniform active sites, and unsaturated coordination configurations.^{4–12} Although numerous studies on SACs have been reported over the past decades,^{13–18} they generally present unsatisfactory apparent activity in many reactions. For instance, it is difficult for SACs to break the linear scaling relationship for the reactions involving multiple steps/intermediates due to the lack of synergistic effects between the neighboring metal atoms.^{19–27} Therefore, it is significant to systematically optimize the activity of SACs by rationally modulating the structure of active sites such as constructing SA-cluster dual sites catalysts, which is also beneficial for an in-depth understanding of the structure–activity relationship at the atomic scale.^{28–40}

Numerous atomically dispersed catalysts (ADs) including SACs have been achieved on various supports such as carbon materials, CeO₂, TiO₂, and Al₂O₃; however, controllably synthesizing silica (SiO₂)-supported ADs with high activity and stability is still challenging due to its “inert” surface.

SiO₂, a typical nonreducible oxide, is widely used as support in both scientific and industrial fields due to its high stability, low cost, nontoxicity, and large specific surface area, which also can afford a clean platform for regulating and understanding the real active sites from the complex catalyst structure.⁴² Nevertheless, to the best of our knowledge, systematically constructing and optimizing atomically dispersed active sites through atom-by-atom fabrication on SiO₂ surfaces has been rarely reported.^{43–47} Therefore, developing a facile and general approach to preparing stable atomically dispersed metal-SiO₂ catalysts is of great necessity.

Herein, we report the controllable construction of SiO₂-supported atomically dispersed Pt₁/SiO₂-N and Pt_{1+n}/SiO₂-N catalysts for the first time by the amino group-assisted atomic layer deposition (ALD) strategy. The key feature of the approach is controlling the uniform and isolated adsorption of Pt precursors (MeCpPtMe₃) on the SiO₂ surface during the

Received: October 1, 2024

Revised: November 25, 2024

Accepted: December 12, 2024

Published: December 20, 2024



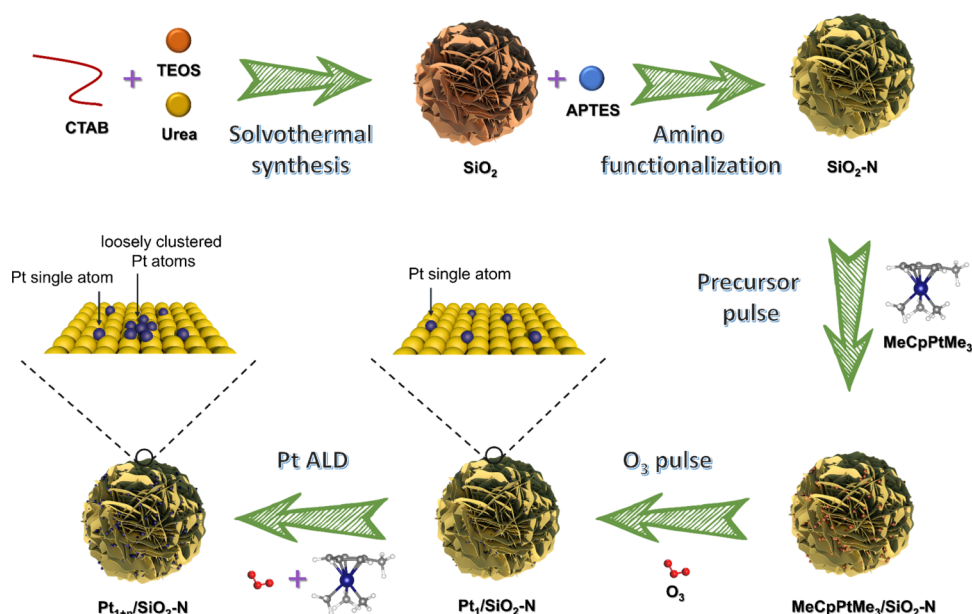


Figure 1. Schematic illustration of the catalyst synthesis (CTAB, TEOS, and APTES represent cetyltrimethylammonium bromide, tetraethyl orthosilicate, and 3-aminopropyltriethoxysilane, respectively).

ALD process to achieve the precise synthesis of atomically dispersed Pt species through atom-by-atom fabrication starting from SACs. Experimental results and density functional theory (DFT) calculations revealed a strong dependence of the catalytic activity and selectivity on the geometric and electronic structures of Pt species. The $\text{Pt}_{1+n}/\text{SiO}_2\text{-N}$ catalysts with SA atomic cluster coexisted dual sites exhibit excellent catalytic activity, stability, and optimized selectivity toward desired haloanilines products (99%). Note that the $\text{Pt}_1/\text{SiO}_2\text{-N}$ catalysts, with the highest atomic utilization efficiency, are almost inactive for the hydrogenation reaction, while the $\text{Pt}_{1+p}/\text{SiO}_2\text{-N}$ catalysts present poor selectivity toward haloanilines. Our present strategy presented here is general and can be potentially extended to synthesizing other SiO_2 -supported metal catalysts with atomic dispersion.

RESULTS AND DISCUSSION

Preparation and Characterization of $\text{Pt}_1/\text{SiO}_2\text{-N}$, $\text{Pt}_{1+n}/\text{SiO}_2\text{-N}$, and $\text{Pt}_{1+p}/\text{SiO}_2\text{-N}$ Catalysts

The dendritic SiO_2 nanoflower sphere was first synthesized by the typical solvothermal method (Figure 1), which possesses a high specific surface area and developed a hierarchical porous structure (Figures 2a, S1, and S2, Supporting Information). The unique structure can not only well confine the Pt species to improve the stability of the catalysts but also enhance the accessibility of reactant molecules to/away from the internal metal. The obtained SiO_2 was then functionalized with 3-aminopropyltriethoxysilane (APTES) named as $\text{SiO}_2\text{-N}$ to provide the adsorption sites for MeCpPtMe_3 precursor molecules. The structure and morphology of nanoflower spheres were well maintained after the amino functionalization process (Figures 2b, S1, and S3, Supporting Information). A series of atomically dispersed catalysts including 0.3 wt % $\text{Pt}_1/\text{SiO}_2\text{-N}$, 0.6 wt % $\text{Pt}_{1+n}/\text{SiO}_2\text{-N}$, and 1.5 wt % $\text{Pt}_{1+p}/\text{SiO}_2\text{-N}$ were successfully synthesized through the atom-by-atom fabrication method starting from SACs by ALD, and the Pt content was determined by inductively coupled plasma optical emission spectrometry (ICP-OES, Table S1, Supporting

information). The key step to construct Pt SAs is that the MeCpPtMe_3 molecules are uniformly adsorbed and bonded with amino groups, and then the second reactant O_3 reacts with MeCpPtMe_3 on the precursor-saturated surface. The Pt species were well controlled by varying the Pt ALD cycles (Figure S4, Supporting information).

The amino functionalization process has a significant influence on the particle size, distribution, and stability of Pt. As revealed by the HAADF-STEM images of Pt/SiO_2 catalysts with as-prepared SiO_2 as supports (Figure 2c,d), the main species are the Pt nanoparticles (Pt_p) coexisted with some SAs, and the many Pt_p are detached from the SiO_2 support even during the sample preparation process (just shaking ca. 5 s in ethanol solution) for transmission electron microscopy (TEM) measurement, indicating the poor stability of the catalysts due to the weak interaction between Pt and SiO_2 . Therefore, the amino functionalization toward SiO_2 is an indispensable step to achieve the high-stability and high-dispersion SiO_2 -based catalyst. Figure 2e shows the typical HAADF-STEM image of 0.3 wt % $\text{Pt}_1/\text{SiO}_2\text{-N}$ catalysts, and the Pt species mainly exist in the form of isolated Pt single atom (Pt_1) with an atomic distance of ca. 0.7 nm and a surface density of about 31 Pt_1 per 100 nm^2 (Figures 2i, S5a–c, and S6a, Supporting information). With the further increase of Pt loading, the 0.6 wt % $\text{Pt}_{1+n}/\text{SiO}_2\text{-N}$ catalysts with Pt_1 and atomic cluster (Pt_n) dual sites are achieved (Figures 2f and S5d–f, Supporting information). As expected, the catalysts show a higher Pt atom density (40 Pt_1 per 100 nm^2 , Figure 2i). Note that the Pt_n is composed of a few loosely assembled atoms still exhibiting atomically dispersed property and that the Pt single atoms of Pt_n are different from that of isolated Pt_1 . The distance of adjacent Pt atoms in Pt_n sites is much shorter than the adjacent distance of Pt atom in $\text{Pt}_1/\text{SiO}_2\text{-N}$, and the corresponding distance of Pt atom in Pt_n is ca. 0.3 nm (Figures 2j–m, S6b, and S7, Supporting Information). Moreover, when the Pt loading is further increased to 1.5 wt %, Pt_p with an average size of 1.1 nm (inset in Figure 2g) is found in the 1.5 wt % $\text{Pt}_{1+p}/\text{SiO}_2\text{-N}$ catalysts (Figures 2g and S5g–i, Supporting Information), and

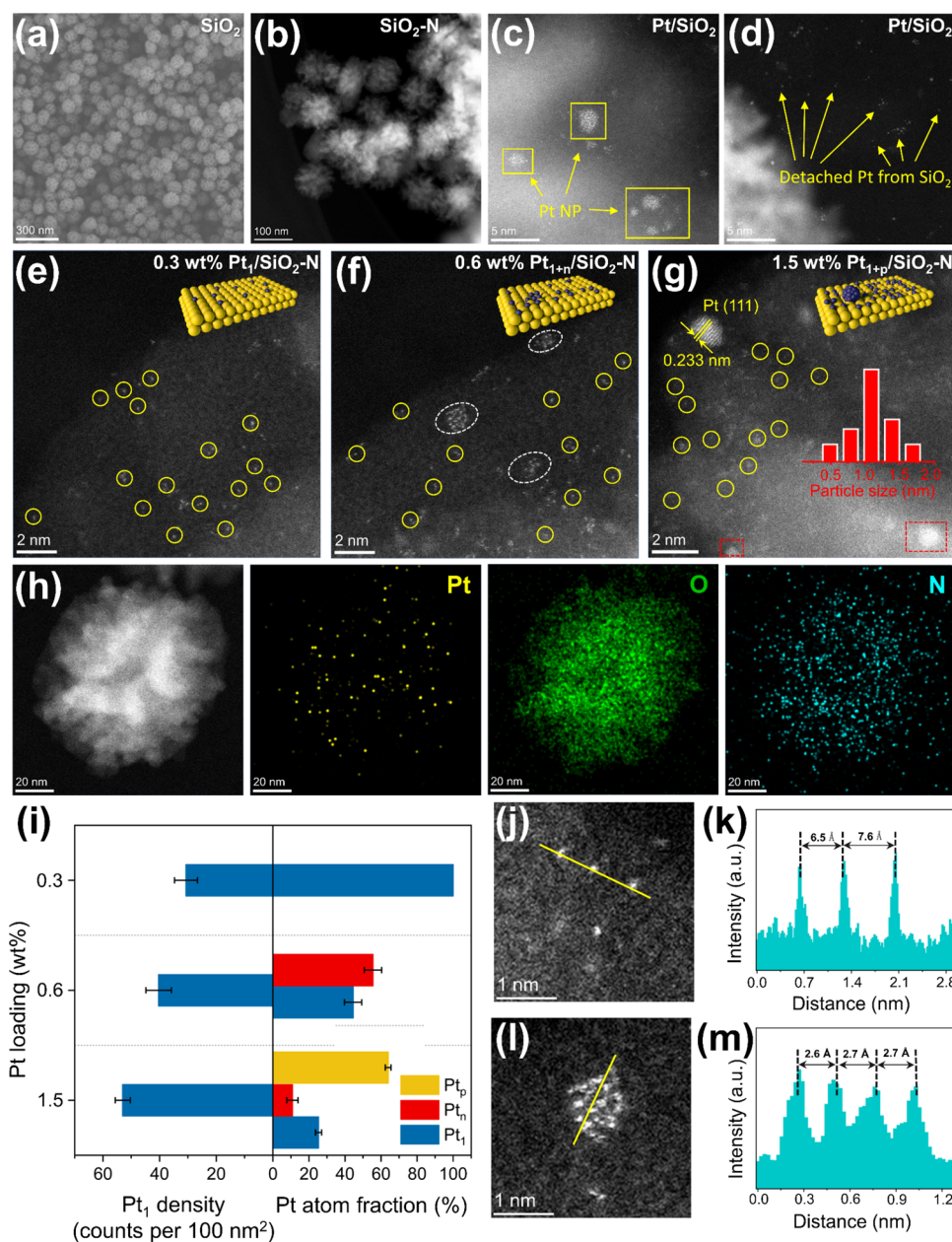


Figure 2. (a) Scanning electron microscopy (SEM) image of SiO_2 . (b) HAADF-STEM image of amino-functionalized $\text{SiO}_2\text{-N}$. High-angle annular dark-field (HAADF)-scanning transmission electron microscopy (STEM) images of (c, d) Pt/SiO_2 , (e) 0.3 wt % $\text{Pt}_1/\text{SiO}_2\text{-N}$, (f) 0.6 wt % $\text{Pt}_{1+n}/\text{SiO}_2\text{-N}$, and (g) 1.5 wt % $\text{Pt}_{1+p}/\text{SiO}_2\text{-N}$ catalysts (inset is the corresponding histogram of particle size distribution and SA is not included). (h) HAADF-STEM and the corresponding elemental mapping images of 0.6 wt % $\text{Pt}_{1+n}/\text{SiO}_2\text{-N}$ catalysts. (i) Statistics of Pt atomic species in 0.3 wt % $\text{Pt}_1/\text{SiO}_2\text{-N}$, 0.6 wt % $\text{Pt}_{1+n}/\text{SiO}_2\text{-N}$, and 1.5 wt % $\text{Pt}_{1+p}/\text{SiO}_2\text{-N}$ catalysts. Pt_1 , Pt_n , and Pt_p stand for Pt single atom, Pt atomic cluster, and Pt nanoparticle, respectively. (j) HAADF-STEM image of 0.3 wt % $\text{Pt}_1/\text{SiO}_2\text{-N}$ and (k) the corresponding line intensity profiles along the yellow lines. (l) HAADF-STEM image of 0.6 wt % $\text{Pt}_{1+n}/\text{SiO}_2\text{-N}$ catalysts and (m) the corresponding line intensity profiles along the yellow lines.

the measured lattice fringe distance of the Pt NPs is approximately 0.223 nm (Figure 2g), which matches well with the Pt(111) plane. Additionally, the Pt NPs can be observed from the low-magnification HAADF-STEM images of 1.5 wt % $\text{Pt}_1/\text{SiO}_2\text{-N}$, while it is not observed from the HAADF-STEM images of 0.3 wt % $\text{Pt}_1/\text{SiO}_2\text{-N}$ and 0.6 wt % $\text{Pt}_{1+n}/\text{SiO}_2\text{-N}$ catalysts (Figure S8, Supporting Information). It is noteworthy that there are still a large amount of Pt_1 (about 53 Pt_1 per 100 nm^2) and Pt_n sites (Figure 2i). Impressively, no detached Pt is observed for the $\text{SiO}_2\text{-N}$ -supported three catalysts, strongly demonstrating the stabilization effect of amino groups toward Pt species. Moreover, there is no

diffraction peak ascribed to Pt species from the X-ray diffraction (XRD) patterns, which again indicates the high dispersion of Pt species in the catalysts (Figure S9, Supporting Information).

To further unravel the physicochemical properties of the catalysts, thorough characterizations were conducted by multiple techniques. The CO absorption-diffuse reflectance infrared Fourier transform (CO-DRIFT) spectroscopy was first adopted to investigate the local structure of catalysts. On the 0.3 wt % $\text{Pt}_1/\text{SiO}_2\text{-N}$ catalysts, no peak can be observed (Figure S10a, Supporting Information). While there is only one very weak peak located at 2093 cm^{-1} for 0.6 wt % $\text{Pt}_{1+n}/$

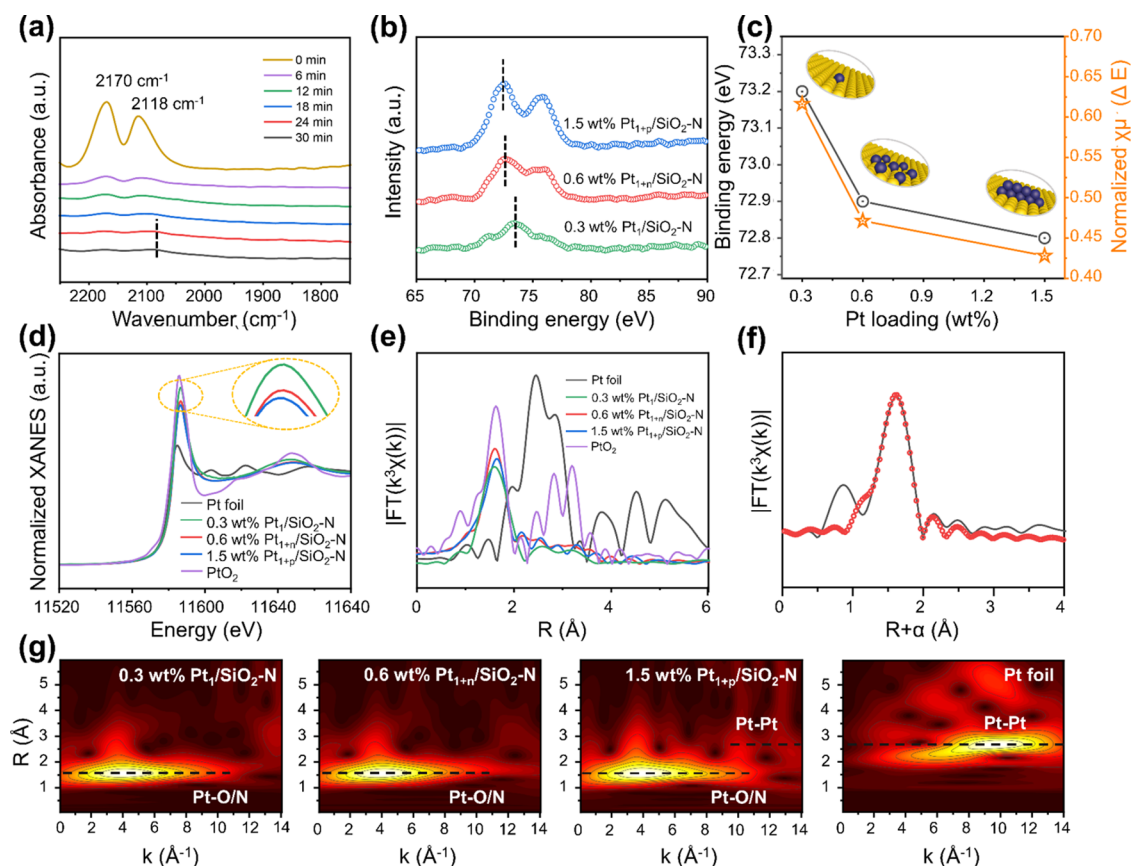


Figure 3. (a) CO–DRIFT spectra of 0.6 wt % $\text{Pt}_{1+n}/\text{SiO}_2\text{-N}$ catalysts. (b) XPS Pt 4f spectra and (c) the corresponding statistics of electronic state Pt over the catalysts. (d) Pt L_3 -edge XANES and (e) EXAFS spectra of the catalysts, Pt foil, and PtO_2 . (f) EXAFS fitting curve of the representative 0.6 wt % $\text{Pt}_{1+n}/\text{SiO}_2\text{-N}$ catalyst. (g) WT-EXAFS spectra of Pt L_3 -edge of the catalysts and Pt foil.

$\text{SiO}_2\text{-N}$ catalysts, assigned to linearly bonded CO on Pt SAs (Figure 3a), again indicating the atomically dispersed property. In contrast, the CO peaks at 2073 cm^{-1} are observed from the spectra of 1.5 wt % $\text{Pt}_{1+p}/\text{SiO}_2\text{-N}$ catalysts, which can be attributed to the linear CO adsorption on metallic Pt nanoparticles/nanocluster,^{48,49} again indicating the existence of Pt_p over the 1.5 wt % $\text{Pt}_{1+p}/\text{SiO}_2\text{-N}$ catalysts, which complies well with the above HAADF-STEM results (Figure S10b, Supporting Information). The spatial intimacy of the Pt atom is expected to have an important influence on the local electronic structure of Pt species (Pt_1 , Pt_n , and Pt_p). To this end, X-ray photoelectron spectroscopy (XPS) spectra of the three catalysts are given (Figures 3b and S11, Supporting Information). For the 0.3 wt % $\text{Pt}_1/\text{SiO}_2\text{-N}$ catalysts with longer atomic distances, the Pt $4f_{7/2}$ possesses the higher binding energy, while the Pt $4f_{7/2}$ of 0.6 wt % $\text{Pt}_{1+n}/\text{SiO}_2\text{-N}$ and 1.5 wt % $\text{Pt}_{1+p}/\text{SiO}_2\text{-N}$ catalysts present apparently lowered binding energies. Moreover, the N 1s peaks at 399.5 eV were also detected from the spectra of the catalysts, again indicating the successful functionalization toward SiO_2 supports, which should play a significant role in stabilizing the Pt species through the potential Pt–N bond.

Similar results are observed in the Pt L_3 -edge X-ray absorption near-edge structure (XANES) spectra. The white-line intensity, reflecting the average oxidation state of Pt, decreases with the increased Pt loading (Figure 3d), indicating that the Pt_1 species are located in cationic states.^{50,51} The white-line intensity of 0.6 wt % $\text{Pt}_{1+n}/\text{SiO}_2\text{-N}$ catalysts is clearly lower than that of 0.3 wt % $\text{Pt}_1/\text{SiO}_2\text{-N}$ catalysts and

close to that of 1.5 wt % $\text{Pt}_{1+p}/\text{SiO}_2\text{-N}$ catalysts due to the synergistic effect of neighboring Pt atoms. The coordination environments of the catalysts were further investigated by the extended X-ray absorption fine structure (EXAFS) spectra, as shown in Figure 3e. For the 0.3 wt % $\text{Pt}_1/\text{SiO}_2\text{-N}$ catalysts, the most noticeable scattering at around 1.5 \AA can be ascribed to the first coordination shell of Pt–O/N (Table S2, Supporting Information), confirming the existence of Pt_1 . Meanwhile, the main peak is still the peak at 1.5 \AA for the 0.6 wt % $\text{Pt}_{1+n}/\text{SiO}_2\text{-N}$ catalysts, indicating that the Pt atoms in the Pt_n existed in the form of few loosely assembled Pt SAs,^{52,53} which is in line with CO–DRIFTS spectra and HAADF-STEM, and it also demonstrated by the EXAFS fitting curve (Figures 3f and S12, Supporting Information). Meanwhile, for the 1.5 wt % $\text{Pt}_{1+p}/\text{SiO}_2\text{-N}$ catalysts, the Pt–Pt scattering path at around 2.5 \AA is quite weak, and the Pt–O/N scattering path can still be observed, which should be due to the partially oxidized property and relatively low crystallinity of ALD-prepared Pt NPs with small size (ca. 1.1 nm); a large number of Pt SAs on 1.5 wt % $\text{Pt}_{1+p}/\text{SiO}_2\text{-N}$ catalysts and detection limit of XAFS still existed.⁵⁴ Similar results can also be seen from the wavelet transforms (WT) of EXAFS (Figure 3g).

Based on the structural analysis results, the 0.3 wt % $\text{Pt}_1/\text{SiO}_2\text{-N}$, 0.6 wt % $\text{Pt}_{1+n}/\text{SiO}_2\text{-N}$, and 1.5 wt % $\text{Pt}_{1+p}/\text{SiO}_2\text{-N}$ catalysts with the corresponding isolated Pt_1 , $\text{Pt}_1 + \text{Pt}_n$, and $\text{Pt}_1 + \text{Pt}_p$ sites were successfully prepared. Note that the obtained Pt_n sites composed of randomly assembled Pt atoms still present atomically dispersed features, which is significantly

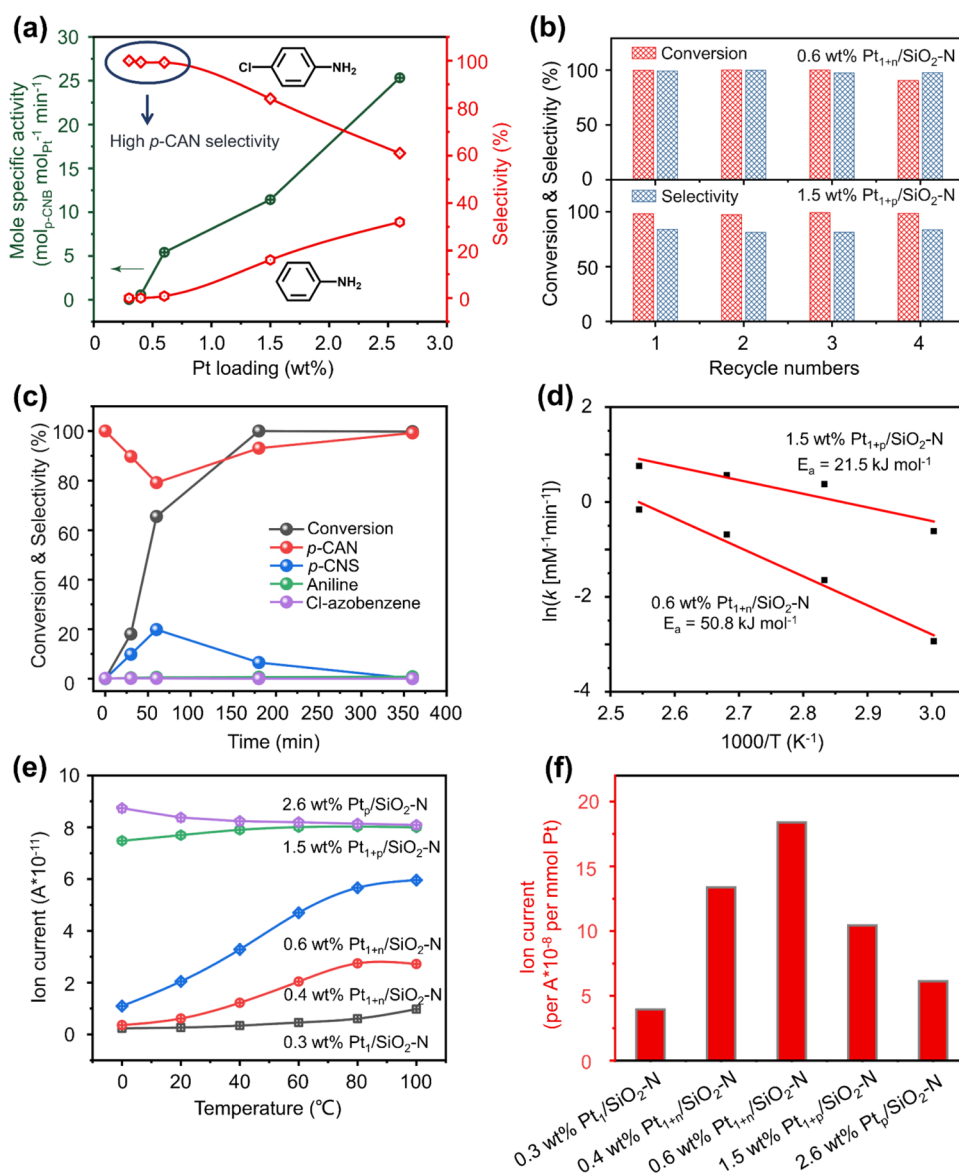


Figure 4. (a) Selective hydrogenation of *p*-CNB over different catalysts. (b) Stability tests of 0.6 wt % Pt_{1+n}/SiO₂-N and 1.5 wt % Pt_{1+p}/SiO₂-N catalysts. (c) Catalytic activity of 0.6 wt % Pt_{1+n}/SiO₂-N catalysts as a function of time. (d) Arrhenius plots of 0.6 wt % Pt_{1+n}/SiO₂-N and 1.5 wt % Pt_{1+p}/SiO₂-N catalyst for hydrogenation of *p*-CNB. (e) TPSRs of H₂ and D₂ over the catalysts at different temperatures (0–100 °C). (f) Formation rate of HD of different catalysts at 80 °C.

different from Pt₁ and Pt_p sites (Figures S5 and S8, Supporting Information). Therefore, the 0.6 wt % Pt_{1+n}/SiO₂-N catalysts with Pt_n sites present a unique electronic and geometric configuration compared with the other two catalysts; i.e., the catalysts not only have the advantages of high atom utilization efficiency and unsaturated coordination structure but also show the property of metallic Pt species, which may lead to unique catalytic properties due to the synergistic effect of spatially intimate Pt atom.

Catalytic Performances of Pt/SiO₂ Catalysts in Selective Hydrogenation

The selective hydrogenation of nitroarenes to produce unsaturated anilines is an important route in the fine chemicals industry. Moreover, it serves as a classic model reaction, benefiting the exploration of structure–activity relationships, an in-depth understanding of catalytic mechanisms, and the identification of active sites. The selective hydrogenation of *p*-

CNB was performed to quantify the catalytic property of the catalysts with different structures (Figure 4a; Tables S3 and S4 Supporting Information). Although the 0.3 wt % Pt₁/SiO₂-N catalyst possesses the highest atomic utilization efficiency, it is almost inactive for the hydrogenation reaction. In contrast, the 0.6 wt % Pt_{1+n}/SiO₂-N catalysts show a much higher mole specific activity ($5.4 \text{ mol}_{p\text{-CNB}} \text{mol}_{\text{Pt}}^{-1} \text{min}^{-1}$) with the selectivity of 99% toward the desired product of *p*-chloroaniline (*p*-CAN) at 99% conversion. The turnover frequency results show a similar tendency with the mole specific activity (Figure S14, Supporting Information). However, for the 1.5 wt % Pt_{1+p}/SiO₂-N catalysts with Pt_p sites, the selectivity to *p*-CAN rapidly decreases to 83%. To further demonstrate the negative impact of Pt_p sites on the selectivity of *p*-CAN, the 2.6 wt % Pt_p/SiO₂-N catalysts with only Pt_p sites were prepared (Figure S15, Supporting Information). The selectivity to *p*-CAN over the catalysts decreased dramatically to 61%, further indicating that Pt_p sites have a detrimental influence on the selectivity of

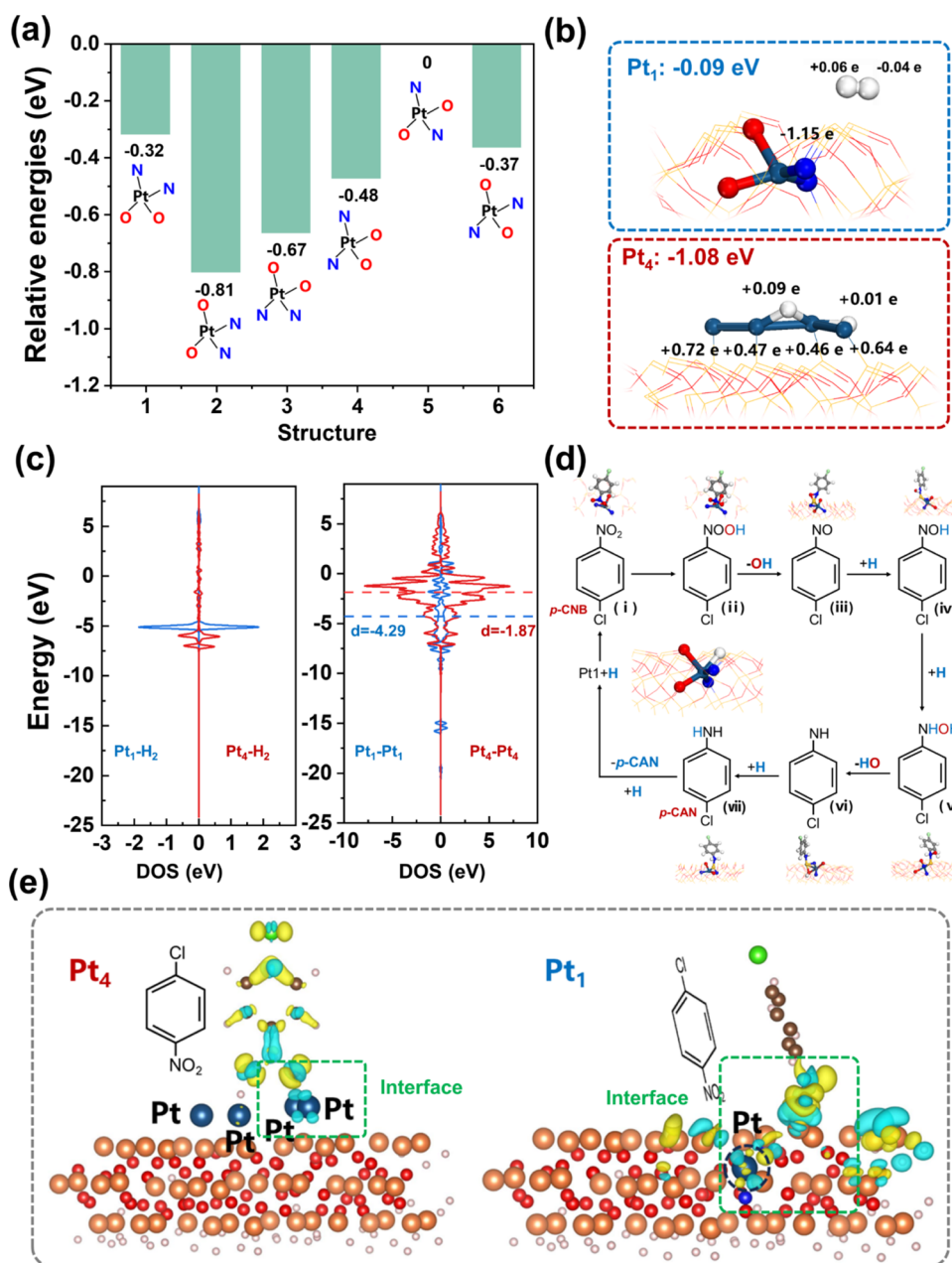


Figure 5. (a) Relative energies of six different single Pt atoms coordinated with two O atoms and two N atoms incorporated into the SiO₂ framework. (b) Electron distribution of H₂ adsorbed on Pt₄ and Pt₁ sites. Blue ball: nitrogen atom; red ball: oxygen atom; dark blue ball: platinum atom; white ball: hydrogen atom. Red and yellow line: SiO₂ support. (c) Total density of states (DOS) of H₂ adsorbed on Pt₄ and Pt₁ sites. (d) Schematic diagram of reaction process of *p*-CNB hydrogenation over Pt₁ sites. (e) Differential charge density plots of *p*-CNB over Pt₄ and Pt₁ sites. The light blue and light yellow isosurfaces represent the decrease and increase of 0.01 eV Å⁻³ charge density, respectively.

the desired products. Moreover, the stability tests of the 0.6 wt % Pt_{1+n}/SiO₂-N and 1.5 wt % Pt_{1+p}/SiO₂-N catalysts were also carried out. The results indicate that the catalysts are quite stable after multiple cyclic tests, without presenting the obvious decrease in view of the activity and structural change (Figures 4b and S16, Supporting Information), while the Pt/SiO₂ catalysts without grafting amino groups exhibit poor stability (Figures S17 and S18, Supporting Information).

Catalytic Mechanism Investigation

In general, the *p*-CNB hydrogenation reaction is divided into dissociation of hydrogen, active hydrogen spillover, and hydrogenation of nitro groups, which is also accompanied by a dechlorination process. The processes could occur on

different active sites or the same one. We further studied the catalytic behavior of different catalysts. For the optimized 0.6 wt % Pt_{1+n}/SiO₂-N catalysts, excellent performance was obtained with 99% selectivity to *p*-CAN at 99% *p*-CNB conversion, and the sequential hydrogenation for *p*-CNB to *p*-CNS, and then to *p*-CAN was observed (Figure 4c). In contrast, for the 1.5 wt % Pt_{1+p}/SiO₂-N catalysts with Pt nanoparticles, the hydrogenation and dechlorination processes occur simultaneously (Figure S19, Supporting Information). Subsequently, the values of apparent activation energy (E_a) are determined to be approximately 50.8 and 21.5 kJ mol⁻¹, respectively, for 0.6 wt % Pt_{1+n}/SiO₂-N and 1.5 wt % Pt_{1+p}/SiO₂-N catalysts (Figure 4d). The attenuated total reflectance

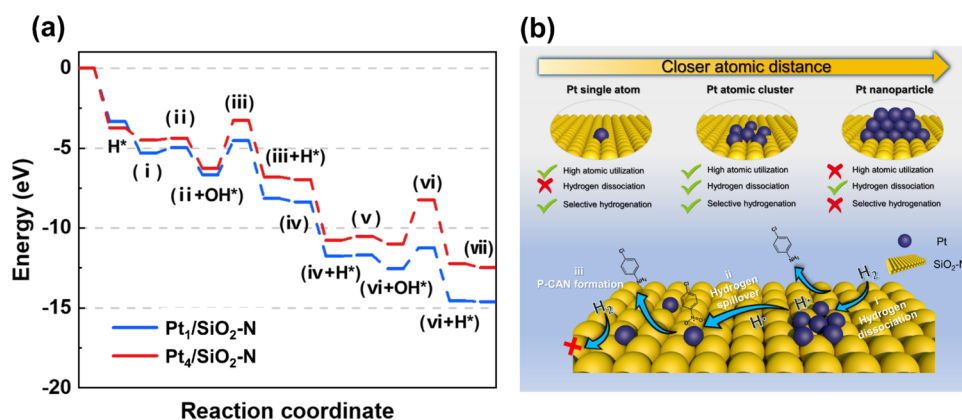


Figure 6. (a) Adsorption energies of different reaction coordinates over Pt_4 and Pt_1 sites. (b) Proposed synergistic catalytic mechanism of dual-site catalyst for nitroarenes selective hydrogenation.

infrared (ATR-IR) spectroscopy was conducted to probe the adsorption of the *p*-CNB substrate (Figure S20, Supporting Information). For the pure *p*-CNB, two bands at 1510 and 1337 cm^{-1} are the asymmetric stretching and symmetric stretching vibrations of the nitro group, respectively, which shift to 1525 and 1345 cm^{-1} when *p*-CNB is adsorbed on 0.3 wt % $\text{Pt}_1/\text{SiO}_2\text{-N}$ catalysts. Similar cases can be found when *p*-CNB is adsorbed on 0.6 wt % $\text{Pt}_{1+n}/\text{SiO}_2\text{-N}$ and 1.5 wt % $\text{Pt}_{1+p}/\text{SiO}_2\text{-N}$ catalysts. The results indicate that the adsorption/activation of *p*-CNB on Pt_1 sites is feasible. Also, control experiments were conducted using ammonia borane as the hydrogen source, and the 0.3 wt % $\text{Pt}_1/\text{SiO}_2\text{-N}$ catalysts could achieve the hydrogenation reaction of *p*-CNB, i.e., a 100% selectivity to *p*-CAN at complete conversion was obtained, again indicating that the Pt_1 should be the potential activation and hydrogenation site of the nitro group (Table S5, Supporting Information). These results indicate that H_2 can be easily dissociated on Pt_n and Pt_p sites generating active hydrogen, while the Pt_n and Pt_1 sites provide the preferential adsorption sites for nitro groups. Note that the hydrogenation and dechlorination processes occur simultaneously on the Pt_p sites due to the existence of multiple sites such as edge, corner, and step,⁵⁵ resulting in the decreased selectivity of *p*-CAN, which can be further demonstrated by control experiments using *p*-CNB and *p*-CAN as the reaction substrates (Figure S21, Supporting Information). The optimized activity and high selectivity of 0.6 wt % $\text{Pt}_{1+n}/\text{SiO}_2\text{-N}$ catalysts can also be verified in the hydrogenation of other nitrobenzene derivatives (Figure S22, Supporting information).

The dissociation of H_2 and the subsequent spillover have important influences on hydrogenation reactions. The temperature-programmed surface reactions (TPSRs) of the mixture of H_2 and D_2 were performed to reveal the nature of hydrogen dissociation ability on Pt species with different structures (Figures 4e and S23–S27, Supporting Information), in which the appearance of HD in the TPSRs suggested the dissociation of H_2 . For the 0.3 wt % $\text{Pt}_1/\text{SiO}_2\text{-N}$ catalysts, the formation rate of HD is only observed at 80 °C with limited activity, which should account for the poor activity of Pt_1 species for hydrogenation of *p*-CNB. In contrast, the formation rates of HD on 0.4 wt % $\text{Pt}_{1+n}/\text{SiO}_2\text{-N}$ and 0.6 wt % $\text{Pt}_{1+n}/\text{SiO}_2\text{-N}$ catalysts containing Pt_n sites are enhanced obviously with the increase of temperatures. Moreover, the 1.5 wt % $\text{Pt}_{1+p}/\text{SiO}_2\text{-N}$ and 2.6 wt % $\text{Pt}_p/\text{SiO}_2\text{-N}$ catalysts exhibit further enhanced apparent hydrogen dissociation ability. For the quantification

of intrinsic activity, the metal normalized activity for hydrogen dissociation at 80 °C was calculated, as shown in Figure 4f. The 0.6 wt % $\text{Pt}_{1+n}/\text{SiO}_2\text{-N}$ catalysts show the highest reaction activity (Table S6, Supporting Information).

Theoretical Perspectives of the Difference in Catalytic Performances

Based on the aforementioned experimental results, we have delineated the distinct roles played by various Pt species in the hydrogenation reactions and obtained the optimized 0.6 wt % $\text{Pt}_{1+n}/\text{SiO}_2\text{-N}$ catalysts with synergistic Pt_1 and Pt_n dual sites. Specifically, atomically dispersed Pt_1 and Pt_n sites exhibit remarkably high selectivity for the hydrogenation of nitro groups, while Pt_p sites demonstrate poor selectivity. Moreover, Pt_n sites display a superior dissociation hydrogenation capability. To gain further deep insights into the synergy between Pt_1 and Pt_n sites in *p*-CNB hydrogenation, we conducted first-principles theoretical calculations utilizing periodic DFT, as depicted in Figure 5. According to the EXAFS results (Figure 2e), six different single Pt atoms coordinated with two O atoms and two N atoms incorporated into the SiO_2 framework were constructed (Figure S28, Supporting Information). It is found that the second single Pt atom exhibits the highest stability, as evidenced by the lowest relative energy (−0.81 eV) in Figure 5a. As a contrast, the Pt_4 sites supported on $\text{SiO}_2\text{-N}$ were also constructed to model Pt_n sites.

The hydrogen adsorption characteristics on Pt_1 and Pt_4 sites supported on $\text{SiO}_2\text{-N}$ were initially investigated (Figure 5b). Notably, Pt_4 sites exhibited a significantly lower adsorption energy of gaseous H_2 than Pt_1 sites (−1.08 < −0.09 eV). This disparity underscores the stronger interaction between Pt_4 sites and H_2 molecules, as evidenced by the dissociative adsorption of gaseous hydrogen on Pt_4 sites and the weak interaction of gaseous hydrogen on Pt_1 sites. After H_2 adsorption on Pt_4 sites, the two H atoms adsorbed on Pt_4 sites gained more electrons (+0.09e and +0.01e) from Pt compared to those adsorbed on Pt_1 sites (+0.06e and −0.04e). For deeper insight into the electronic structure, we computed the density of states (DOS) of H_2 adsorbed on different Pt_4 and Pt_1 sites (Figure 5c). The broader peaks in the DOSs of H_2 on the Pt_4 sites emphasize the stronger electronic interaction between the Pt_4 sites and H_2 . Additionally, the average d-band center of Pt_4 sites, closer to the Fermi level than that of Pt_1 sites (−1.87 > −4.29), underscores the higher activation activity of H_2 on Pt_4 sites. These results demonstrate that Pt_4 sites are more favorable for

the dissociative adsorption of hydrogen, which is in accordance with the experimental results (Figure 4f).

The entire reaction process of *p*-CNB hydrogenation over Pt₁ and Pt₄ to form *p*-CAN is illustrated in Figures 5d and S29, Supporting Information. Initially, H₂ dissociates from Pt₄ sites to form two H atoms which are then further adsorbed by Pt₄ and adjacent Pt₁ sites.⁵⁶ In comparison to Pt₁ sites, Pt₄ sites exhibit a higher adsorption energy for H proton (−3.7 < −3.3 eV). Subsequently, reactants *p*-CNB adsorb on both the Pt₄ and Pt₁ sites. Notably, the adsorption energy of *p*-CNB on Pt₁ sites is lower than that on Pt₄ sites (−1.99 < 0.76 eV). Differential charge density plots (Figure 5e) illustrate stronger electrical interactions at the interfaces of Pt₁ sites and *p*-CNB, indicating the enhanced activation of *p*-CNB on Pt₁ sites. The adsorption energy profiles in different reaction coordinates (Figure 6a) reveal that Pt₁ sites follow a lower-energy reaction path than Pt₄ sites during *p*-CNB hydrogenation. Consequently, the aforementioned experimental and DFT calculations suggest that Pt_n sites are advantageous for H₂ adsorption and dissociation to form H proton, while Pt₁ sites are favorable for *p*-CNB hydrogenation with H proton (Figure 6b). The synergistic interplay between Pt₁ and Pt_n sites should elucidate the exceptional overall activity of 0.6 wt % Pt_{1+n}/SiO₂–N catalysts. Meanwhile, the dynamic stability of Pt₁ and Pt_n sites was investigated through systematic AIMD simulations at 353 K. From the results, the structure of the Pt₁ and Pt₄ sites remain stable throughout the simulation process (Figure S30).

CONCLUSIONS

In summary, we achieve the controllable synthesis of atomically dispersed Pt species over SiO₂ by the amino group-assisted ALD strategy and unravel the strong dependence of *p*-CNB hydrogenation activity and selectivity on the size of Pt species. Especially, the Pt_{1+n}/SiO₂–N catalysts with stable Pt₁ and Pt_n dual sites exhibit optimized selectivity toward *p*-CAN due to the remarkable synergy of dual sites, which can dissociate hydrogen via the Pt_n species and preferentially activate nitro groups with the help of nearby Pt₁ species to generate *p*-CAN. In contrast, the isolated Pt₁ site is almost inactive for hydrogen dissociation. Nitro and chlorine groups can be simultaneously activated on the Pt_p sites due to the existence of multiple sites, which results in poor selectivity toward *p*-CAN. The present strategy can be potentially applied to other SiO₂-supported metal catalysts with atomic dispersion, and the unique design of dual sites will afford new guidance for the atomically dispersed catalysts with high efficiency.

METHODS

Preparation of Dendritic Mesoporous SiO₂

Typically, cetyltrimethylammonium bromide (CTAB), sodium dodecyl sulfate (SDS), and triethanolamine (TEAH₃) were dissolved in H₂O and stirred for an hour at 80 °C. After that, the tetraethyl orthosilicate (TEOS) was added to the mixture and continued stirring for 2 h at 80 °C. The molar ratio is 1.0 TEOS:0.06 CTAB:0.02 SDS:0.026 TEAH₃:80 H₂O. Afterward, a whitish solid was collected by centrifugation, washed with water and ethanol three times, respectively, and dried at 60 °C for 12 h. The products were calcined at 750 °C in air for 6 h to obtain dendritic mesoporous SiO₂.

Preparation of SiO₂–N

1 g of dendritic mesoporous SiO₂ was dispersed in 100 mL of toluene with stirring in a three-neck flask at 80 °C, and then 5 mL of 3-aminopropyltriethoxysilane (APTES) was added into the solution,

which was continuously stirred at 80 °C for 48 h. After that, the suspension was centrifuged with ethanol and water three times, respectively. Finally, the samples were dried by a vacuum freeze-dryer to obtain the SiO₂–N.

Preparation of Pt/SiO₂–N Catalysts

First, the functionalized SiO₂–N was dispersed on a quartz wafer and dried at room temperature in air. Pt species were then deposited onto SiO₂–N by using a homemade hot-wall, closed-chamber ALD reactor. Pt ALD was performed by sequentially exposing the SiO₂–N to MeCpPtMe₃ and ozone (O₃), which served as the Pt precursor and oxidant, respectively. The deposition temperature was set at 250 °C, and MeCpPtMe₃ was maintained at 60 °C. Ultrahigh-purity N₂ (99.999%) was used as the carrier and purge gas. The Pt structure and loading were controlled by adjusting the Pt ALD cycles, obtaining 0.3 wt % Pt₁/SiO₂–N (10 cycles), 0.6 wt % Pt_{1+n}/SiO₂–N (30 cycles), and 1.5 wt % Pt_{1+p}/SiO₂–N (50 cycles) catalysts. For comparison, Pt/SiO₂ catalysts with original SiO₂ as the support were also prepared using the same method.

ASSOCIATED CONTENT

Data Availability Statement

The data that support the findings of this study are available from the corresponding author upon reasonable request.

Supporting Information

The Supporting Information is available free of charge at <https://pubs.acs.org/doi/10.1021/jacsau.4c00924>.

Detailed experimental section; characterization methods; and additional material characterization (DOCX)

AUTHOR INFORMATION

Corresponding Authors

Xiang Feng – State Key Laboratory of Heavy Oil Processing, China University of Petroleum, Qingdao 266580, China; Email: xiangfeng@upc.edu.cn

Yong Qin – Interdisciplinary Research Center of Biology and Catalysis, School of Life Sciences, Northwestern Polytechnical University, Xi'an 710072, China; State Key Laboratory of Coal Conversion, Institute of Coal Chemistry, Chinese Academy of Sciences, Taiyuan 030001, China; Email: qinyong@nwpu.edu.cn

Jiankang Zhang – Interdisciplinary Research Center of Biology and Catalysis, School of Life Sciences, Northwestern Polytechnical University, Xi'an 710072, China; orcid.org/0000-0003-4483-8107; Email: zhangjiankang@nwpu.edu.cn

Authors

Hao Xu – School of Chemistry and Chemical Engineering, Northwestern Polytechnical University, Xi'an 710072, China; Interdisciplinary Research Center of Biology and Catalysis, School of Life Sciences, Northwestern Polytechnical University, Xi'an 710072, China

Dong Lin – Max Planck-Cardiff Centre on the Fundamentals of Heterogeneous Catalysis FUNCAT, Cardiff Catalysis Institute, School of Chemistry, Cardiff University, Cardiff CF103AT, U.K.; orcid.org/0000-0001-5313-8204

Jie Shi – Qingyuan Innovation Laboratory, Quanzhou 362801, China; orcid.org/0000-0002-8993-3258

Zhengxing Lv – Shanghai Synchrotron Radiation Facility, Shanghai Advanced Research Institute, Chinese Academy of Sciences, Shanghai 201204, China

Xinshuo Zhao – Interdisciplinary Research Center of Biology and Catalysis, School of Life Sciences, Northwestern Polytechnical University, Xi'an 710072, China

Linge Ning – Interdisciplinary Research Center of Biology and Catalysis, School of Life Sciences, Northwestern Polytechnical University, Xi'an 710072, China

Jiao Xiao – Interdisciplinary Research Center of Biology and Catalysis, School of Life Sciences, Northwestern Polytechnical University, Xi'an 710072, China

Lin Cui – Interdisciplinary Research Center of Biology and Catalysis, School of Life Sciences, Northwestern Polytechnical University, Xi'an 710072, China

Jian Zhang – School of Chemistry and Chemical Engineering, Northwestern Polytechnical University, Xi'an 710072, China; State Key Laboratory of Solidification Processing and School of Materials Science and Engineering, Northwestern Polytechnical University, Xi'an 710072, China

Juncong Yuan – State Key Laboratory of Heavy Oil Processing, China University of Petroleum, Qingdao 266580, China

Complete contact information is available at:
<https://pubs.acs.org/10.1021/jacsau.4c00924>

Author Contributions

◆ H.X., D.L., J.S., and Z.L. authors contributed equally. H.X.: data curation, formal analysis, investigation, writing—original draft, writing—review and editing; D.L.: data curation, formal analysis, investigation; J.S.: data curation, formal analysis, investigation; Z.L.: data curation, formal analysis, investigation; X.Z.: data curation, investigation; L.N.: data curation, investigation; J.X.: data curation, investigation; L.C.: data curation, investigation; J.Z.: review and editing; J.Y.: data curation, investigation; X.F.: review and editing; Y.Q.: review and editing; J.Z.: conceptualization, data curation, formal analysis, funding acquisition, investigation, methodology, project administration, resources, writing—original draft, writing—review and editing.

Notes

The authors declare no competing financial interest.

ACKNOWLEDGMENTS

We appreciate the financial support from the National Natural Science Foundation of China (22372130 and 22102131) and Fundamental Research Funds for the Central Universities (24GH0201184 and G2023KY0605). We appreciate the Analytical & Testing Center of Northwestern Polytechnical University for HAADF-STEM measurements and Shanghai Synchrotron Radiation Facility for XAFS measurements (BL11B).

REFERENCES

- (1) Johnson, N. J. J.; Lam, B.; MacLeod, B. P.; Sherbo, R. S.; Moreno-Gonzalez, M.; Fork, D. K.; Berlinguette, C. P. Facets and vertices regulate hydrogen uptake and release in palladium nanocrystals. *Nat. Mater.* **2019**, *18*, 454–458.
- (2) Christopher, P.; Linic, S. Engineering selectivity in heterogeneous catalysis: Ag nanowires as selective ethylene epoxidation catalysts. *J. Am. Chem. Soc.* **2008**, *130*, 11264–11265.
- (3) Zhang, J.; Yu, Z.; Gao, Z.; Ge, H.; Zhao, S.; Chen, C.; Chen, S.; Tong, X.; Wang, M.; Zheng, Z.; Qin, Y. Porous TiO₂ nanotubes with spatially separated platinum and CoO_x cocatalysts produced by atomic layer deposition for photocatalytic hydrogen production. *Angew. Chem., Int. Ed.* **2017**, *56*, 816–820.

- (4) Chen, Y.; Zhao, J.; Pan, X.; Li, L.; Yu, Z.; Wang, X.; Ma, T.; Lin, S.; Lin, J. Tuning the inter-metal interaction between Ni and Fe Atoms in dual-atom catalysts to boost CO₂ electroreduction. *Angew. Chem., Int. Ed.* **2024**, *63*, No. e202411543.

- (5) Bruix, A.; Lykhach, Y.; Matolínová, I.; Neitzel, A.; Skála, T.; Tsud, N.; Vorokhta, M.; Stetsovych, V.; Ševčíková, K.; Mysliveček, J.; Fiala, R.; Václavů, M.; Prince, K. C.; Bruyère, S.; Potin, V.; Illas, F.; Matolín, V.; Libuda, J.; Neyman, K. M. Maximum noble-metal efficiency in catalytic materials: atomically dispersed surface platinum. *Angew. Chem., Int. Ed.* **2014**, *53*, 10525–10530.

- (6) Li; Huang, X.; Liu, B. Catalyst: single-atom catalysis: directing the way toward the nature of catalysis. *Chem* **2019**, *5*, 2733–2735.

- (7) Malta, G.; Kondrat, S. A.; Freakley, S. J.; Davies, C. J.; Lu, L.; Dawson, S.; Thetford, A.; Gibson, E. K.; Morgan, D. J.; Jones, W.; Wells, P. P.; Johnston, P.; Catlow, C. R. A.; Kiely, C. J.; Hutchings, G. J. Identification of single-site gold catalysis in acetylene hydrochlorination. *Science* **2017**, *355*, 1399–1403.

- (8) Hülsey, M. J.; Zhang, B.; Ma, Z.; Asakura, H.; Do, D. A.; Chen, W.; Tanaka, T.; Zhang, P.; Wu, Z.; Yan, N. In situ spectroscopy-guided engineering of rhodium single-atom catalysts for CO oxidation. *Nat. Commun.* **2019**, *10*, No. 1330.

- (9) Wang, L.; Chen, M.; Yan, Q.; Xu, S.; Chu, S.; Chen, P.; Lin, Y.; Liang, H. A sulfur-tethering synthesis strategy toward high-loading atomically dispersed noble metal catalysts. *Sci. Adv.* **2019**, *5*, No. eaax6322.

- (10) Gawande, M. B.; Ariga, K.; Yamauchi, Y. Single-atom catalysts. *Small* **2021**, *17*, No. 2101584.

- (11) Cui, T.; Wang, Y.; Ye, T.; Wu, J.; Chen, Z.; Li, J.; Lei, Y.; Wang, D.; Li, Y. Engineering dual single-atom sites on 2D ultrathin n-doped carbon nanosheets attaining ultra-low-temperature zinc-air battery. *Angew. Chem., Int. Ed.* **2022**, *61*, No. e202115219.

- (12) Kong, F.; Liu, X.; Song, Y.; Qian, Z.; Li, J.; Zhang, L.; Yin, G.; Wang, J.; Su, D.; Sun, X. Selectively coupling Ru single atoms to PtNi concavities for high-performance methanol oxidation via d-band center regulation. *Angew. Chem., Int. Ed.* **2022**, *61*, No. e202207524.

- (13) Li, J.; Jiang, Y.; Wang, Q.; Xu, C.; Wu, D.; Banis, M. N.; Adair, K. R.; Doyle-Davis, K.; Meira, D. M.; Finrock, Y. Z.; Li, W.; Zhang, L.; Sham, T.; Li, R.; Chen, N.; Gu, M.; Li, J.; Sun, X. A general strategy for preparing pyrrolic-N₄ type single-atom catalysts via pre-located isolated atoms. *Nat. Commun.* **2021**, *12*, No. 6806.

- (14) Yang, M.; Li, S.; Wang, Y.; Herron, J. A.; Xu, Y.; Allard, L. F.; Lee, S.; Huang, J.; Mavrikakis, M.; Flytzani-Stephanopoulos, M. Catalytically active Au-O(OH)_x-species stabilized by alkali ions on zeolites and mesoporous oxides. *Science* **2014**, *346*, 1498–1501.

- (15) Wang, C.; Mao, S.; Wang, Z.; Chen, Y.; Yuan, W.; Ou, Y.; Zhang, H.; Gong, Y.; Wang, Y.; Mei, B.; Jiang, Z.; Wang, Y. Insight into single-atom-induced unconventional size dependence over CeO₂-supported Pt catalysts. *Chem* **2020**, *6*, 752–765.

- (16) Yang, X.-F.; Wang, A.; Qiao, B.; Li, J.; Liu, J.; Zhang, T. Single-atom catalysts: a new frontier in heterogeneous catalysis. *Acc. Chem. Res.* **2013**, *46*, 1740–1748.

- (17) Kunwar, D.; Zhou, S.; DeLaRiva, A.; Peterson, E. J.; Xiong, H.; Pereira-Hernández, X. I.; Purdy, S. C.; ter Veen, R.; Brongersma, H. H.; Miller, J. T.; Hashiguchi, H.; Kovarik, L.; Lin, S.; Guo, H.; Wang, Y.; Datye, A. K. Stabilizing high metal loadings of thermally stable platinum single atoms on an industrial catalyst support. *ACS Catal.* **2019**, *9*, 3978–3990.

- (18) Gu, J.; Jian, M.; Huang, L.; Sun, Z.; Li, A.; Pan, Y.; Yang, J.; Wen, W.; Zhou, W.; Lin, Y.; Wang, H.; Liu, X.; Wang, L.; Shi, X.; Huang, X.; Cao, L.; Chen, S.; Zheng, X.; Pan, H.; Zhu, J.; Wei, S.; Li, W.; Lu, J. Synergizing metal-support interactions and spatial confinement boosts dynamics of atomic nickel for hydrogenations. *Nat. Nanotechnol.* **2021**, *16*, 1141–1149.

- (19) Yao, D.; Wang, Y.; Li, Y.; Li, A.; Zhen, Z.; Lv, J.; Sun, F.; Yang, R.; Luo, J.; Jiang, Z.; Wang, Y.; Ma, X. Scalable synthesis of Cu clusters for remarkable selectivity control of intermediates in consecutive hydrogenation. *Nat. Commun.* **2023**, *14*, No. 1123.

- (20) Zhang, Z.; Tian, J.; Lu, Y.; Yang, S.; Jiang, D.; Huang, W.; Li, Y.; Hong, J.; Hoffman, A. S.; Bare, S. R.; Engelhard, M. H.; Datye, A.

- K.; Wang, Y. Memory-dictated dynamics of single-atom Pt on CeO₂ for CO oxidation. *Nat. Commun.* **2023**, *14*, No. 2664.
- (21) Kuai, L.; Chen, Z.; Liu, S.; Kan, E.; Yu, N.; Ren, Y.; Fang, C.; Li, X.; Li, Y.; Geng, B. Titania supported synergistic palladium single atoms and nanoparticles for room temperature ketone and aldehydes hydrogenation. *Nat. Commun.* **2020**, *11*, No. 48.
- (22) Liu, L.; Meira, D. M.; Arenal, R.; Concepcion, P.; Puga, A. V.; Corma, A. Determination of the evolution of heterogeneous single metal atoms and nanoclusters under reaction conditions: which are the working catalytic sites. *ACS Catal.* **2019**, *9*, 10626–10639.
- (23) Xie, S.; Liu, L.; Lu, Y.; Wang, C.; Cao, S.; Diaio, W.; Deng, J.; Tan, W.; Ma, L.; Ehrlich, S. N.; Li, Y.; Zhang, Y.; Ye, K.; Xin, H.; et al. Pt atomic single-layer catalyst embedded in defect-enriched ceria for efficient CO oxidation. *J. Am. Chem. Soc.* **2022**, *144*, 21255–21266.
- (24) Ding, K.; Gulec, A.; Johnson, A. M.; Schweitzer, N. M.; Stucky, G. D.; Marks, L. D.; Stair, P. C. Identification of active sites in CO oxidation and water-gas shift over supported Pt catalysts. *Science* **2015**, *350*, 189–192.
- (25) Zhang, J.; Yang, H.; Liu, B. Coordination engineering of single-atom catalysts for the oxygen reduction reaction: a review. *Adv. Energy Mater.* **2021**, *11*, No. 2002473.
- (26) Guan, E.; Gates, B. C. Stable rhodium pair sites on MgO: influence of ligands and rhodium nuclearity on catalysis of ethylene hydrogenation and H-D exchange in the reaction of H₂ with D₂. *ACS Catal.* **2018**, *8*, 482–487.
- (27) Chen, S.; Gong, B.; Gu, J.; Lin, Y.; Yang, B.; Gu, Q.; Jin, R.; Liu, Q.; Ying, W.; Shi, X.; Xu, W.; Cai, L.; Li, Y.; Sun, Z.; Wei, S.; Zhang, W.; Lu, J. Dehydrogenation of ammonia borane by platinum-nickel dimers: regulation of heteroatom interspace boosts bifunctional synergistic catalysis. *Angew. Chem.* **2022**, *134* (41), No. e202211919.
- (28) Zhang, L.; Meng, G.; Zhang, W.; Li, X.; Zhang, Z.; Yang, M.; Wu, Y.; Wang, D.; Li, Y. Oriented conversion of a LA/HMF mixture to GVL and FDCA in a biphasic solvent over a Ru single-atom/nanoparticle dual-site catalyst. *ACS Catal.* **2023**, *13*, 2268–2276.
- (29) Fu, N.; Liang, X.; Wang, X.; Gan, T.; Ye, C.; Li, Z.; Liu, J.; Li, Y. Controllable conversion of platinum nanoparticles to single atoms in Pt/CeO₂ by laser ablation for efficient CO oxidation. *J. Am. Chem. Soc.* **2023**, *145*, 9540–9547.
- (30) Hu, C.; Hu, J.; Zhu, Z.; Lu, Y.; Chu, S.; Ma, T.; Zhang, Y.; Huang, H. Orthogonal charge transfer by precise positioning of silver single atoms and clusters on carbon nitride for efficient piezocatalytic pure water splitting. *Angew. Chem., Int. Ed.* **2022**, *61*, No. e202212397.
- (31) Boronat, M.; Leyva-Pérez, A.; Corma, A. Theoretical and experimental insights into the origin of the catalytic activity of subnanometric gold clusters: attempts to predict reactivity with clusters and nanoparticles of gold. *Acc. Chem. Res.* **2014**, *47*, 834–844.
- (32) Ye, T.-N.; Xiao, Z.; Li, J.; Gong, Y.; Abe, H.; Niwa, Y.; Sasase, M.; Kitano, M.; Hosono, H. Stable single platinum atoms trapped in sub-nanometer cavities in 12CaO·7Al₂O₃ for chemoselective hydrogenation of nitroarenes. *Nat. Commun.* **2020**, *11*, No. 1020.
- (33) Zhang, J.; Gao, Z.; Wang, S.; Wang, G.; Gao, X.; Zhang, B.; Xing, S.; Zhao, S.; Qin, Y. Origin of synergistic effects in bicomponent cobalt oxide-platinum catalysts for selective hydrogenation reaction. *Nat. Commun.* **2019**, *10*, No. 4166.
- (34) Lin, J.; Ding, J.; Wang, H.; Yang, X.; Zheng, X.; Huang, Z.; Song, W.; Ding, J.; Han, X.; Hu, W. Boosting energy efficiency and stability of Li-CO₂ batteries via synergy between Ru atom clusters and single-atom Ru-N₄ sites in the electrocatalyst cathode. *Adv. Mater.* **2022**, *34*, No. 2200559.
- (35) Zhang, J.; Pan, Y.; Feng, D.; Cui, L.; Zhao, S.; Hu, J.; Wang, S.; Qin, Y. Mechanistic insight into the synergy between platinum single atom and cluster dual active sites boosting photocatalytic hydrogen evolution. *Adv. Mater.* **2023**, *35*, No. 2300902.
- (36) Zhang, J.; Wang, M.; Gao, Z.; Qin, X.; Xu, Y.; Wang, Z.; Zhou, W.; Ma, D. Importance of species heterogeneity in supported metal catalysts. *J. Am. Chem. Soc.* **2022**, *144*, 5108–5115.
- (37) Liu, H.; Lang, X.; Zhu, C.; Timoshenko, J.; Rüscher, M.; Bai, L.; Guijarro, N.; Yin, H.; Peng, Y.; Li, J.; Liu, Z.; Wang, W.; Cuenya, B. R.; Luo, J. Efficient electrochemical nitrate reduction to ammonia with copper-supported rhodium cluster and single-atom catalysts. *Angew. Chem., Int. Ed.* **2022**, *61*, No. e202202556.
- (38) Wang, H.; Liu, J.; Allard, L. F.; Lee, S.; Liu, J.; Li, H.; Wang, J.; Wang, J.; Oh, S. H.; Li, W.; et al. Surpassing the single-atom catalytic activity limit through paired Pt-O-Pt ensemble built from isolated Pt₁ atoms. *Nat. Commun.* **2019**, *10*, No. 3808.
- (39) Zhao, Y.; Kumar, P. V.; Tan, X.; Lu, X.; Zhu, X.; Jiang, J.; Pan, J.; Xi, S.; Yang, H. Y.; Ma, Z.; Wan, T.; Chu, D.; Jiang, W.; Smith, S. C.; Amal, R.; Han, Z.; Lu, X. Modulating Pt-O-Pt atomic clusters with isolated cobalt atoms for enhanced hydrogen evolution catalysis. *Nat. Commun.* **2022**, *13*, No. 2430.
- (40) Ao, X.; Zhang, W.; Li, Z.; Li, J.; Soule, L.; Huang, X.; Chiang, W.; Chen, H. M.; Wang, C.; Liu, M.; Zeng, X. C. Markedly enhanced oxygen reduction activity of single-atom Fe catalysts via integration with Fe nanoclusters. *ACS Nano* **2019**, *13*, 11853–11862.
- (41) Lang, R.; Du, X.; Huang, Y.; Jiang, X.; Zhang, Q.; Guo, Y.; Liu, K.; Qiao, B.; Wang, A.; Zhang, T. Single-atom catalysts based on the metal-oxide interaction. *Chem. Rev.* **2020**, *120*, 11986–12043.
- (42) Zhang, D.; Cai, H.; Su, Y.; Sun, W.; Yang, D.; Ozin, G. A. Silica samurai: aristocrat of energy and environmental catalysis. *Chem. Catal.* **2022**, *2*, 1893–1918.
- (43) Zhang, S.; Tang, Y.; Nguyen, L.; Zhao, Y.; Wu, Z.; Goh, T.; Liu, J. J.; Li, Y.; Zhu, T.; Huang, W.; Frenkel, A. I.; Li, J.; Tao, F. F. Catalysis on singly dispersed Rh atoms anchored on an inert support. *ACS Catal.* **2018**, *8*, 110–121.
- (44) Mora-Raimundo, P.; Lozano, D.; Benito, M.; Mulero, F.; Manzano, M.; Vallet-Regí, M. Osteoporosis remission and new bone formation with mesoporous silica nanoparticles. *Adv. Sci.* **2021**, *8*, No. 2101107.
- (45) Yun, J.; Wang, W.; Kim, S. M.; Bae, T.; Lee, S.; Kim, D.; Lee, G.; Lee, H.; Song, M. Light trapping in bendable organic solar cells using silica nanoparticle arrays. *Energy Environ. Sci.* **2015**, *8*, 932–940.
- (46) Huang, H.; Mao, M.; Zhang, Q.; Li, Y.; Bai, J.; Yang, Y.; Zeng, M.; Zhao, X. Solar-light-driven CO₂ reduction by CH₄ on silica-cluster-modified Ni nanocrystals with a high solar-to-fuel efficiency and excellent durability. *Adv. Energy Mater.* **2018**, *8*, No. 1702472.
- (47) Zhang, T. Single-atom catalysis: far beyond the matter of metal dispersion. *Nano Lett.* **2021**, *21*, 9835–9837.
- (48) Dong, C.; Gao, Z.; Li, Y.; Peng, M.; Wang, M.; Xu, Y.; Li, C.; Xu, M.; Deng, Y.; Qin, X.; Huang, F.; Wei, X.; Wang, Y.-G.; Liu, H.; Zhou, W.; Ma, D. Fully exposed palladium cluster catalysts enable hydrogen production from nitrogen heterocycles. *Nat. Catal.* **2022**, *5*, 485–493.
- (49) Sun, G.; Zhao, Z. J.; Mu, R.; Zha, S.; Li, L.; Chen, S.; Zang, K.; Luo, J.; Li, Z.; Purdy, S. C.; Kropf, A. J.; Miller, J. T.; Zeng, L.; Gong, J. Breaking the scaling relationship via thermally stable Pt/Cu single atom alloys for catalytic dehydrogenation. *Nat. Commun.* **2018**, *9*, No. 4454.
- (50) Jeong, H.; Shin, S.; Lee, H. Heterogeneous atomic catalysts overcoming the limitations of single-atom catalysts. *ACS Nano* **2020**, *14*, 14355–14374.
- (51) Shin, S.; Haaring, R.; So, J.; Choi, Y.; Lee, H. Highly durable heterogeneous atomic catalysts. *Acc. Chem. Res.* **2022**, *55*, 1372–1382.
- (52) Wei, H.; Liu, X.; Wang, A.; Zhang, L.; Qiao, B.; Yang, X.; Huang, Y.; Miao, S.; Liu, J.; Zhang, T. FeO_x-supported platinum single-atom and pseudo-single-atom catalysts for chemoselective hydrogenation of functionalized nitroarenes. *Nat. Commun.* **2014**, *5*, No. 5634.
- (53) Ke, J.; Zhu, W.; Jiang, Y.; Si, R.; Wang, Y.; Li, S.; Jin, C.; Liu, H.; Song, W.; Yan, C.; Zhang, Y. Strong local coordination structure effects on subnanometer PtO_x clusters over CeO₂ nanowires probed by low-temperature CO oxidation. *ACS Catal.* **2015**, *5*, 5164–5173.
- (54) Finzel, J.; Sanroman Gutierrez, K. M.; Hoffman, A. S.; Resasco, J.; Christopher, P.; Bare, S. R. Limits of Detection for EXAFS Characterization of Heterogeneous Single-Atom Catalysts. *ACS Catal.* **2023**, *13*, 6462–6473.
- (55) Zhang, S.; Chang, C.; Huang, Z.; Li, J.; Wu, Z.; Ma, Y.; Zhang, Z.; Wang, Y.; Qu, Y. High catalytic activity and chemoselectivity of

sub-nanometric Pd clusters on porous nanorods of CeO₂ for hydrogenation of nitroarenes. *J. Am. Chem. Soc.* **2016**, *138*, 2629–2637.

(56) Gu, K.; Lin, S. Sustained hydrogen spillover on Pt/Cu(111) single-atom alloy: dynamic insights into gas-induced chemical processes. *Angew. Chem., Int. Ed.* **2023**, *62*, No. e202312796.